Vibrational predissociation dynamics of the $He^{79}Br_2$ van der Waals molecule: A quantum mechanical study

Cite as: J. Chem. Phys. **105**, 7454 (1996); https://doi.org/10.1063/1.472573
Submitted: 03 June 1996 . Accepted: 22 July 1996 . Published Online: 31 August 1998

Tomás González-Lezana, Marta I. Hernández, Gerardo Delgado-Barrio, Alexei A. Buchachenko, and Pablo Villarreal

Vibrational predissociation dynamics of the $He^{79}Br_2$ van der Waals molecule: A quantum mechanical study

Tomás González-Lezana, Marta I. Hernández, Gerardo Delgado-Barrio, Alexei A. Buchachenko,[a] and Pablo Villarreal
Instituto de Matemáticas y Física Fundamental (C.S.I.C.), Serrano 123, E-28004-Madrid, Spain

(Received 3 June 1996; accepted 22 July 1996)

The vibrational predissociation of the $HeBr_2$ van der Waals complex is studied by means of both accurate and approximate three dimensional quantum mechanical calculations. Simple atom–atom potentials have been tested for matching experimental measurements at low Br_2 vibrational excitations. The fragmentation dynamics when the bromine subunit is close to its B state dissociation limit is then explored and compared with experiments. For low to intermediate vibrational states v, good agreement with most of the data (spectral shifts, lifetimes, average structures, average product energies) is achieved. The closing of the $\Delta v=-1$ channel at $v=44$ and the binding energy at that position are successfully reproduced, although calculated and experimental blueshifts and linewidths are not in such good accordance in the $v>38$ range. For these high v excitations, fragmentation cross sections exhibit complicated structures indicating strong interactions among different quasibound states. In addition, interesting threshold and intramolecular energy redistribution effects are predicted. The closing of the $\Delta v=-1$ channel is found to be a gradual process where different dynamical regimes can be investigated in detail. [S0021-9606(96)03040-1]

I. INTRODUCTION

The dynamics of rare gas–halogen van der Waals (vdW) molecules is an important subject since energy transfer mechanisms can be deeply investigated–both experimentally and theoretically—at the state-to-state level. These molecules, formed by a halogen or interhalogen molecule BC weakly bound to a rare gas atom X, undergo vibrational predissociation (VP) after being excited with a laser pulse from the ground (X) to an excited electronic state (B)

$$\mathrm{X}\cdots\mathrm{BC}(X)\xrightarrow{h\nu}\mathrm{X}\cdots\mathrm{BC}^*(B,v)\xrightarrow{\mathrm{VP}}\mathrm{X}+\mathrm{BC}^*(B,v'<v), \tag{1.1}$$

where v labels the vibrational state of BC. Many experiments have been carried out for different rare gases (He,Ne,Ar) bound to molecules such as I_2,[1–3] Cl_2,[4–6] and ICl,[7–9] and a broad variety of behavior has been found, ranging from vibrational to translational (V–T) energy transfer [as in HeI_2 (Ref. 10)] to intramolecular vibrational redistribution (IVR) [as in $ArCl_2$ (Ref. 6)], including processes where energy transfer to the rotational degrees of freedom is important (as in NeICl,[8] for example). Moreover, a wide range of dynamical behavior can be sampled for a single molecule by varying the vibrational excitation v in the quasibound state.[11] Theoretical work has contributed to understand these processes, establishing useful propensity rules[12,13] and developing approximate[14,15] as well as three-dimensional[16,17] quantum mechanical treatments.

One of the main conclusions of these studies is that simple atom–atom additive potential models are able to reproduce well most of the experimental results. In particular, an atom–atom form for the rare gas–homonuclear halogen interaction gives T-shaped average structures, which are consistent with almost all the available spectroscopic data.[2,4] This is an important finding, given the difficulty in obtaining accurate *ab initio* potential energy surfaces for these many-electron systems. Some of the few *ab initio* calculations, however, have led one to suspect that the minimum of the potential well is not in the perpendicular configuration but in the linear one.[18–20] One interesting example is $HeCl_2$ in the X electronic state:[21] although an *ab initio*-based potential has its deepest point in the linear configuration, a secondary minimum in the perpendicular configuration with a smaller curvature causes the ground vdW state wave function to be localized around the perpendicular configuration. Thus, the ground vdW state is not essentially different to the one obtained using some simple atom–atom model potential. If fact, an atom–atom potential has been found to fit quite well a large amount of spectroscopic information.[4,22] It could be said that pairwise model potentials give a reasonable representation for the study of VP in rare gas–halogen molecules. However, more work is needed to determine potential energy surfaces, either using more rigorous semiempirical procedures, such as the diatomic-in-molecule based ones,[23] or through *ab initio* calculations.

One system for which there is a rather large experimental information but not too many theoretical studies is $HeBr_2$. van de Burgt *et al.*[24] have carried out laser induced fluorescence studies for transitions from $HeBr_2(X, v=0)$ to the quasibound states $HeBr_2(B,v)$, $v=11$–38, reporting vibrational predissociation rates and spectral (blue) shifts. More recently, Jahn *et al.*[25] have studied a higher range of vibrational diatomic states ($v=34$–48) using the pump–probe spectroscopic technique. An intriguing behavior in the VP

[a]Permanent address: Department of Chemistry, Moscow State University, Moscow 119899, Russia.

dynamics was found for vibrational states close to the Br_2 dissociation limit ($v \geqslant 40$): For these vibrational levels, spectral shifts were found to decrease substantially, displaying an erratic behavior as v increases. The authors suggest that, for such a large Br–Br separation, the He–Br interaction might change substantially, the vdW bond becoming stronger. On the other hand, they found that for excitations to the $v=45$ state and higher, the $\Delta v=-1$ channel for VP is closed, i.e., the vdW bond energy is larger than the difference between the $v=45$ and $v=44$ Br_2 levels. Sharfin *et al.*[11] observed similar behavior for the HeI_2 complex, although the dependency of both predissociation rates and spectral shifts on v was found to be much smoother than in the $HeBr_2$ case. There are also recent data for linewidths and blueshifts for the low v region, $v=8$–12.[26] Analysis of the rotational bands in all the experimental studies has been found to be consistent with rigid T-shaped geometries for both the ground and the excited electronic states. So far, a detailed analysis of the product distributions has been precluded because of the small rotational constants of the Br_2 fragment. Sivakumar *et al.*[27] have studied the partitioning of energy between the rotational and translational degrees of freedom by simulation of the unresolved rotational bands with a Boltzmann population distribution. They concluded that VP in $HeBr_2$ is mostly a V–T process.

Theoretical studies were also performed in the recent work of Jahn *et al.*[26] They used Morse atom–atom potentials (for the short range part of the He–Br interaction) for the B state and tested two potentials, not having an atom–atom form, for the X state. They found that the more anisotropic potential for the X state gave a very good fit to the main (rotationally resolved) excitation band of $v=8$. The analytic form of this potential was originally proposed by Huang *et al.*[21] to fit MP4 points (calculated using Moller–Plesset perturbation theory to fourth order) for the $HeCl_2(X)$ system. In the experimental work a secondary band was also observed which was attributed to the promotion to excited vdW modes of $HeBr_2(B)$. With the interaction potentials used in that work, the calculated vdW excited state band was only in qualitative agreement with the experimental one. Jahn *et al.* also carried out ''Golden Rule'' calculations for studying the VP dynamics of low v levels. The calculated spectral shifts and VP rates were in good agreement with experimental data in the range studied, $v=8$–20.

In this paper, we study the fragmentation dynamics of the $He^{79}Br_2(B,v)$ complex over a wide range of vibrational excitations, covering all the experimental measurements ($v=8$–46). The aim of this work is to test simple model potentials by comparison against experimental data referred to above. For both the X and B electronic states, additive He–Br Morse potentials were fitted to reproduce, at low vibrational excitations of bromine, several experimental magnitudes such as spectral shifts, lifetimes, and average structures. With these model potentials, calculations are extended to investigate the $HeBr_2$ dissociation dynamics near the $Br_2(B)$ dissociation limit, where experiments found the most interesting dynamical behavior. Full three-dimensional (3D) quantum mechanical calculations[17] are carried out to obtain resonance line shapes, lifetimes, averaged structures, spectral shifts, and final product distributions. Also, the validity of the Golden Rule approximation is assessed by comparing with the more accurate 3D quantum calculations at low and moderately high v values. We find that, with these simple interaction potentials, most of the experimental measurements up to $v \approx 38$ are satisfactorily reproduced. For higher v excitations, deviations from pure Lorentzian line shapes and appearance of overlapped resonances (suggesting the onset of intramolecular vibrational energy redistribution[28]) are noticed. Although calculated blueshifts do not show the same trend encountered experimentally, the simulated spectra in the region of the partial closing of the $\Delta v=-1$ channel is found in qualitative accordance with the recorded one. Possible sources of the discrepancies with the experimental data are indicated and discussed. The investigation of IVR processes presumably appearing in the fragmentation dynamics near the Br_2 dissociation limit certainly deserves further attention. This will be a subject of future work.

The paper is organized as follows. In Sec. II, the basic equations are formulated. The fitting procedure of the potential energy surface is outlined in Sec. III. In Sec. IV, results are reported and discussed. Finally, conclusions are given in Sec. V.

II. THEORY

A. Three-dimensional quantal (line shape) calculations

In this section, the basic equations for the three-dimensional quantal line shape calculations are briefly reviewed. A detailed account of this theory is given elsewhere.[17] The partial cross section for excitation from an initial bound state i of $HeBr_2(X)$ to a final continuum state f of $He+Br_2(B)$ is given (within first order perturbation theory) by

$$\sigma_{f\leftarrow i}(E)=\frac{4\pi^2\omega}{c}\left|\langle\Psi_{fE}(B)|\boldsymbol{\mu}\cdot\mathbf{e}|\Psi_i(X)\rangle\right|^2, \tag{2.1}$$

where ω and $\mathbf{e}$ are the angular frequency and the polarization vector of the incident photon, $\boldsymbol{\mu}$ is the transition dipole moment of the system for the electronic transition, $\Psi_i(X)$ and $\Psi_{fE}(B)$ are the bound and dissociative nuclear wave functions with energies E_i and E, respectively, and $E=E_i+\hbar\omega$. In Eq. (2.1), f assembles the quantum numbers v' (vibrational) and j' (rotational) of the diatomic fragment.

For both electronic states (X and B), the Hamiltonian for the molecular system in Jacobi coordinates can be written as (assuming that reduced wave functions $\Psi=rR\Psi'$ are being used)

$$H^{\epsilon}=-\frac{\hbar^2}{2m}\frac{\partial^2}{\partial R^2}-\frac{\hbar^2}{2\mu}\frac{\partial^2}{\partial r^2}+\frac{\mathbf{l}^2}{2mR^2}+\frac{\mathbf{j}^2}{2\mu r^2}+V^{\epsilon}_{Br_2}(r)+W^{\epsilon}_{HeBr_2}(r,R,\theta), \tag{2.2}$$

where $\mathbf{r}$ is the vector joining the two Br nuclei and $\mathbf{R}$ is the vector from the center of mass of Br_2 to the helium nucleus, respectively, and θ is the angle between $\mathbf{r}$ and $\mathbf{R}$. The re-

duced masses of Br_2 and $HeBr_2$ are μ and m, while **l** and **j** are angular momenta associated with the vectors **R** and **r**, respectively. $V^{\epsilon}_{Br_2}$ and $W^{\epsilon}_{HeBr_2}$ are intramolecular and vdW intermolecular interaction potentials for the ground ($\epsilon=X$) and excited ($\epsilon=B$) electronic states.

The initial bound, $\Psi_i(X)$, and the final continuum, $\Psi_{fE}(B)$, wave functions are expanded as follows:

$$\Psi_i^{(JMp_ip_j)(X)}=\sum_{v,k,j,\Omega} a^i_{vkj\Omega}\varphi_k(R)\chi^X_v(r)\Theta^{(JMp_ip_j)(B)}_{j\Omega}(\hat{\mathbf{r}},\hat{\mathbf{R}}), \tag{2.3}$$

$$\Psi_{fE}^{(JMp_ip_j)(B)}=\sum_{v,j,\Omega} \phi^{fE}_{vj\Omega}(R)\chi^B_v(r)\Theta^{(JMp_ip_j)(B)}_{j\Omega}(\hat{\mathbf{r}},\hat{\mathbf{R}}). \tag{2.4}$$

In Eq. (2.3), $\varphi_k(R)$ is a numerical basis set obtained by solving a suitable one-dimensional reference Hamiltonian. In Eqs. (2.3) and (2.4), $\chi^{\epsilon}_v(r)$ ($\epsilon=X,B$) are wave functions obtained by numerically solving the one dimensional Schrödinger equation

$$\left[-\frac{\hbar^2}{2\mu}\frac{\partial^2}{\partial r^2}+V^{\epsilon}_{Br_2}(r)\right]\chi^{\epsilon}_v=E^{\epsilon}_v\chi^{\epsilon}_v. \tag{2.5}$$

On the other hand, $\Theta^{JMp_ip_j}_{j\Omega}$ is a free rotor basis set in the body-fixed frame (where the z axis is parallel to **R**)

$$\Theta^{JMp_ip_j}_{j\Omega}=[2(1+\delta_{\Omega 0})]^{-1/2}[\Phi^{JM}_{j\Omega}+p_i(-1)^J\Phi^{JM}_{j-\Omega}], \tag{2.6}$$

which is an eigenfunction of the operator of coordinate inversion, with eigenvalue $p_i=\pm 1$. In Eq. (2.6), $\Phi^{JM}_{j\Omega}$ is given as the appropriate product of Wigner and spherical harmonic functions,[17] J is the quantum number associated with the total angular momentum $\mathbf{J}=\mathbf{l}+\mathbf{j}$, and M and Ω are projections of **J** onto the space and body fixed z axes, respectively. As the halogen molecule studied here is homonuclear, the rotational basis also includes the label p_j, the parity under nuclei exchange; $p_j=+1$ or -1 when the quantum number j is even or odd, respectively. Total wave functions [Eqs. (2.3) and (2.4)] are built as linear combinations of rotational functions with either even or odd j's, to have the correct parity.

Line shape calculations are performed as follows. First, the initial bound function $\Psi_i^{(JMp_ip_j)(X)}$ is obtained by diagonalization of the H^X Hamiltonian matrix. Second, to obtain the final dissociative wave function $\Psi_{fE}^{(JMp_ip_j)(B)}$, the expansion given in Eq. (2.4) is introduced into the Schrödinger equation corresponding to the Hamiltonian for $\epsilon=B$ [Eq. (2.2)], leading to a close coupled system for the set of unknown functions $\phi^{fE}_{vj\Omega}$ depending on the dissociative coordinate R. Such close-coupled equations are solved at each energy E by means of a Numerov propagator[29] and applying the appropriate boundary conditions.[17] The quadrature involved in Eq. (2.1) is carried out by accumulation at the same time that the propagation is performed.[30] A parallel transition is assumed, i.e., the transition dipole moment $\boldsymbol{\mu}$ lies along the halogen internuclear axis. In addition, dependency of $\boldsymbol{\mu}$ on the internuclear distance r is neglected. Selection rules for this kind of transitions are:[4,17] $p_i(X)\neq p_i(B)$, $p_j(X)\neq p_j(B)$, and $\Delta J=0,\pm 1$ (with $J=0\rightarrow 0$ forbidden).

The total cross section, which gives the photofragmentation line shape as a function of E, is

$$\sigma_i(E)=\sum_f \sigma_{f\leftarrow i}(E), \tag{2.7}$$

with the rovibrational distribution of the fragments given by

$$P^{(i)}_f(E)=\frac{\sigma_{f\leftarrow i}(E)}{\sigma_i(E)}. \tag{2.8}$$

B. Golden rule calculations

For low vibrational diatomic states it is expected that the Franck–Condon factors will strongly favor the transition between the initial state $\Psi_i(X)$ and a quasibound state $\Psi^q_v(B)$ which eventually decays to final continuum states $\Psi_{fE}(B)$ via the weak coupling induced by the potential term W^B. In this context, the molecular Hamiltonian in the B state can be approximated by

$$\begin{aligned} H&\approx \mathscr{H}_{(v)}+\mathscr{H}_{(v'<v)}+\mathscr{W}_{\text{coup}},\\ \mathscr{H}_{(v)}&=|\chi_v\rangle H_{v,v}\langle\chi_v|,\\ \mathscr{H}_{(v'<v)}&=\sum_{v'<v}|\chi_{v'}\rangle H_{v',v'}\langle\chi_{v'}|,\\ \mathscr{W}_{\text{coup}}&=\sum_{v'<v}|\chi_v\rangle H_{v,v'}\langle\chi_{v'}|, \end{aligned} \tag{2.9}$$

where $H_{v,v'}=\langle\chi_v|H|\chi_{v'}\rangle$. The decay rate of the zero-order state, $\Psi^q_v(B)=\chi^B_v\psi^q_v$ (where ψ^q_v is a discrete eigenstate of $H_{v,v}$ with eigenvalue E^q_v), to the dissociative state $\Psi_{fE}(B)$ is given within Fermi's Golden Rule approximation by the partial half-width

$$\Gamma_f=\pi|\langle\Psi^q_v|\mathscr{W}_{\text{coup}}|\Psi_{fE}\rangle|^2, \tag{2.10}$$

where Ψ_{fE} is an eigenfunction of $\mathscr{H}_{(v'<v)}$ on the energy shell, i.e., $E=E^q_v$. In this situation, it is proved[12] that the partial photodissociation cross section exhibits a pure Lorentzian line shape with a maximum at $E_v\approx E^q_v$, and a half-width $\Gamma=\Sigma_f\Gamma_f$. In this approach, the final product distribution is $P_f=\Gamma_f/\Gamma$.

To obtain the Golden Rule rate, the wave function Ψ^q_v is calculated using the same procedure as for the X state wave function [Eq. (2.3)] for the particular vibrational channel v of the B state. The dissociative wave function Ψ_{fE}, which corresponds asymptotically to $He+Br_2(B,v'<v,j')$, is computed using the expansion of Eq. (2.4) where only vibrational channels $v'<v$ are included.

III. POTENTIAL ENERGY SURFACE AND FITTING PROCEDURE

The potential energy surface is constructed as a sum of pairwise Br–Br and Br–He interactions. For the X state intramolecular interaction, $V^X_{Br_2}$, a Morse potential was em

TABLE I. Parameters of the $HeBr_2$ (X,B) potential energy surfaces.

		D (cm^{-1})	α ($Å^{-1}$)	ρ_e (Å)
Br–Br	X	24 557.674	1.588	2.281
	B	RKR potential (Ref. 32)		
He–Br	X	19.62	1.55	3.81
	B	17.00	1.55	3.92

ployed where the equilibrium distance r_e was taken from available data[31] and D and α were chosen to reproduce the tabulated vibrational constants w_e and $w_e x_e$.[31] For the B state of Br_2, the RKR potential extracted from spectroscopy data by Barrow *et al.*[32] was used.

The intermolecular interactions are assumed to be given by a sum of Morse functions for both electronic states $\epsilon=X,B$

$$W^{\epsilon}_{HeBr_2}(r,R,\theta)=D^{\epsilon}\sum_{i=1,2}\{\exp[-2\alpha^{\epsilon}(\rho_i-\rho_e^{\epsilon})] - 2\exp[-\alpha^{\epsilon}(\rho_i-\rho_e^{\epsilon})]\}, \tag{3.1}$$

where $\rho_{1,2}=[R^2+(r/2)^2\pm Rr\cos\theta]^{1/2}$ are the distances from He to each bromine nucleus.

The fitting procedure of the Morse parameters is as follows. The goal is to achieve a global agreement with experiments for low to moderately high diatomic states. First, an initial set of D^B, α^B, and ρ_e^B was chosen to roughly reproduce, by means of Golden Rule calculations, the experimental linewidth as well as the He to Br_2 center of mass average distance for the level $v=8$.[26] This last magnitude is defined as

$$\overline{R^B}(v=8)=(\langle\Psi_v^q|R^{-2}|\Psi_v^q\rangle)^{-1/2}. \tag{3.2}$$

Golden Rule calculations for several diatomic vibrational states ($v=8$–30) were performed for slight variations of the parameters D^B and α^B, in order to obtain an overall agreement with the experimental lifetimes.[24,26] Dependence of the quasibound state energy E_v^q with v was checked against the experimental blueshifts [the spectral shift is just $E_v^q(B)-E_i(X)$]. Next, X state parameters were adjusted: ρ_e^X in the same way as that described above for the ρ_e^B parameter (using $v_X=0$); D^X and α^X to reproduce the spectral shifts. Line shape calculations were carried out at selected v values to check the validity of Golden Rule calculations. For $v\geqslant 28$, some deviations were noticed mainly for the blueshifts. Hence, line shape calculations were used to make the last refinement of the D^B and α^B parameters.

The final choice for the vdW potential parameters is presented in Table I, together with the parameters of the Br_2 intramolecular potential. With these potentials, the He–Br_2 average distances are $R^X(v_X=0)=3.977$ Å and $R^B(v=8)=4.117$ Å, in good agreement with those obtained by fitting rigid rotor parameters to the observed spectra, $R^X_{rr}(v_X=0)=3.98\pm 0.03$ Å and $R^B_{rr}(v=8)=4.11\pm 0.02$ Å, respectively.

TABLE II. Vibrational and rotational channels included in the close-coupling expansion of Eq. (2.4).

v	Vibrational channels	Rotational channels
10, 20–26	$(v-3,\ldots,v+2)$	$j=0,2,\ldots,34$
28–34	$(v-3,\ldots,v+2)$	$j=0,2,\ldots,26$
36–46	$(v-4,\ldots,v+3)$	$j=0,2,\ldots,22$

IV. RESULTS AND DISCUSSION

Three-dimensional line shape calculations (hereafter referred as ''LS calculations'') for $He^{79}Br_2$ have been conducted for the transition

$$HeBr_2(X,v_X,n_X,1^-_-)\xrightarrow{h\nu}HeBr_2^*(B,v,n,0^+_+) \rightarrow[He+Br_2^*(v'<v,j')](B,0^+_+), \tag{4.1}$$

where the eigenvalues of the symmetry operators are indicated in the notation $J^{p_i}_{p_j}$ for both electronic states.[4] The v and n labels are approximate quantum numbers associated with the Br_2 stretch and the vdW modes, respectively. In Eq. (4.1), $v_X=0$, $n_X=0$, and $n=0$. Calculations within the Golden Rule approximation (hereafter referred as ''GR calculations'') were also performed to study the decay of the $HeBr_2^*(B,v,n=0,0^+_+)$ quasibound state for low v values.

A. Numerical details

LS calculations were conducted for excitations to diatomic levels $v=10,20$–46. The rotational and vibrational channels included in the expansion of the dissociative wave functions [Eq. (2.4)] are listed in Table II. For the X bound state calculation [see Eq. (2.3)], the basis set is composed of two vibrational channels ($v_X=0,1$), eight numerical functions $\varphi_k(R)$, and 18 rotor functions. In the GR calculations, on the other hand, for $v=8$–32, three vibrational ($v-3$,$v-2$,$v-1$) and 18 rotational channels were included in the computation of the continuum wave functions. The basis set for computing the quasibound state $[\Psi_v^q(B)]$ was similar to that used for the X state calculation. In both LS and GR calculations, close coupled equations were integrated from 1.0 to 18.5 Å with a total number of 1024 steps. The angular dependence of the X and B vdW potentials was taken into account using expansions of 35 even Legendre polynomials. Reduced masses of Br_2 and He–Br_2 were taken as 39.459 15 and 3.903 61 a.m.u., respectively. Convergence checks were run within both GR and LS approaches. For $v=24$, for instance, accuracy for the resonance energies and linewidths is better than 10^{-2} cm^{-1}, and product distributions are converged within less than 2%. LS cross sections exhibit pure Lorenztian profiles for $v<36$. Positions E and half-widths Γ of the VP resonances are obtained by fitting a Lorentzian function to the calculated line shape. For $36\leqslant v\leqslant 40$, deviations in the calculated profiles from a Lorentzian shape were observed; such deviations become very large for $v>40$. Thus, for high diatom excitations, only crude estimations of positions and widths were possible; hence accuracy in those

TABLE III. Calculated line shape and Golden Rule spectral shifts and half-widths (in cm^{-1}), obtained with the model potential used in this work. In the last column, Golden Rule results of Jahn *et al.* (Ref. 26), corresponding to a different interaction potential, are also presented for comparison.

		This work		Ref. 26
v		L. shape	G. Rule	G. Rule
8	Shift:	⋯	3.72	3.72
	Γ:	⋯	0.013	0.013
10		3.78	3.77	3.76
		0.018	0.019	0.018
12		⋯	3.81	3.80
		⋯	0.027	0.024
16		⋯	3.92	3.89
		⋯	0.054	0.040
20		4.07	4.06	4.00
		0.094	0.096	0.065
24		4.22	4.23	⋯
		0.168	0.167	⋯
28		4.37	4.45	⋯
		0.275	0.264	⋯
32		4.50	4.75	⋯
		0.430	0.386	⋯

magnitudes is poorer than that achieved for lower excitations (this point is further discussed in Sec. IV D).

B. Low Br_2 vibrational levels

GR and LS results are compared to estimate the range of validity of the Golden Rule approximation. In addition, the potential model presented here is compared with a recent potential proposed by Jahn *et al.*[26] which reproduces well most of the VP data for low v levels. Finally, product distributions are reported and discussed in light of studies on this[27] or related[4,35] vdW systems. In Sec. IV D, our results on spectral shifts and half-widths are tested against measurements for the full v range, including those levels studied here.

In Table III we present LS and GR results of half-widths Γ as well as spectral shifts $E_v(B)-E_i(X)$. Also in Table III, GR calculations of Jahn *et al.*[26] with a different potential model are collected. $E(B,v)$ and $E_i(X)$ are vdW energies considered respect to the $He+Br_2(B,v)$ and $He+Br_2(X, v_X=0)$ dissociation limits, respectively. The computed energy of the $HeBr_2$ ground state was $E_i(X)=-17.573\ cm^{-1}$, which is within the experimental estimation, $-17.0\pm1.5\ cm^{-1}$.[25] Comparing LS and GR calculations (see the two first columns in Table III), it can be seen that both approaches yield almost identical results up to $v=24$. For $v>24$, GR blueshifts deviate from the LS ones towards higher values. This is a consequence of neglecting (in the GR approach) bound–bound coupling terms which become more important as v increases, since anharmonicity in the Br_2 stretch mode makes smaller the energy separation among zero order states of different v manifolds. GR half-widths, on the other hand, lie below the LS ones for $v\geqslant24$. This fact can be understood in light of the energy gap law:[12] as GR approach gives higher resonance energies than the LS ones, fragment kinetic energies are larger giving a more important energy mismatch and thus, a slower VP rate. Here on, it is understood that results presented in this work have been obtained within the GR approach if $v<20$. If $v\geqslant20$, results correspond to LS calculations.

In Table III our GR results are also compared with GR calculations done with a somewhat different B state potential (see Table I of Ref. 26). Apart from slight variations in the Morse parameters describing the atom–atom interactions, the distinct feature of that potential is the inclusion of the proper long range vdW behavior. As can be seen, both potentials yield very similar results for the three lowest levels studied, $v=8,10,12$. At $v=16$ and 20, the potential proposed here systematically leads to higher values of the two magnitudes, shifts and Γ's, than those of Ref. 26. Actually, differences are more important in the half-widths than in the shifts [our calculated Γ's are 35% ($v=16$) and 48% ($v=20$) larger than the Jahn *et al.*'s ones, for instance]. As will be shown later, our potential fits reasonably well experimental widths up to $v=40$. Since the difference in this magnitude produced by the two potentials seems to increase with v, it is expected that the potential of Ref. 26 would yield too small linewidths for high v excitations.

At $v=8$, Jahn *et al.*[26] observed a second excitation band which was assigned to the excitation of vdW bending modes. We have computed the $(X,\ v=0,\ n=0)\rightarrow(B,\ v=8,\ n\neq0)$ excitation spectra, finding narrow peaks at -7.95, -6.41, -5.38, and $-4.11\ cm^{-1}$ with respect to the $He+Br_2(B,\ v=8)$ dissociation limit. Their positions could give the correct band shift but too low intensities are predicted. With the present interaction potential, B excited and X ground vdW states do not overlap sufficiently enough to yield a more important absorption intensity. Similar conclusions were reached in this regard by Jahn *et al.*,[26] who computed the whole range of relevant rotational transitions.

Rotational distributions of the Br_2 fragments in vibrational states $v'=8,9$ upon dissociation of $HeBr_2(B,\ v=10)$ are shown in Table IV. Also Table IV, the projection of the initial quasibound state $\Psi^q_{v=10}$ onto the product (free rotor) basis is also displayed. Populations of the $\Delta v=-3,-2,-1$ vibrational channels are 0.06%, 2.47%, and 97.47% of the total, respectively. This vibrational distribution is in accordance with experiments performed on the same v level,[27] where it was estimated that the ratio between the $v'=8$ and $v'=9$ populations is less than 5%. Unfortunately, detailed product distributions have not been measured for this or other v levels, because the probe laser linewidth is not narrow enough to resolve the product spectra. Nevertheless, Sivakumar *et al.*[27] have estimated the average product rotational energy assuming a Boltzmann distribution which fits the unresolved rotational band. Although they found deviations in the spectrum from the calculated Boltzmann distribution, average rotational energy was considered to be a good estimation. They obtained $\langle E_{rot}(v'=9)\rangle=2\ cm^{-1}$ for the same transition studied here, which compares reasonably well with our result, $\langle E^{calc}_{rot}(v'=9)\rangle=\Sigma_{j'}P'_{j',v'}B_{v'}j'(j'+1)=1.55\ cm^{-1}$ ($P'_{j',v'}$ are normalized to the v' channel, i.e., $\Sigma_{j'}P'_{j',v'}=1$). Rotational energy is only 1.3% of the

TABLE IV. Second column: decomposition of the $HeBr_2$ $(B,v=10)$ quasibound state onto a free rotor basis. Third and fourth columns: product $Br_2(B,v=9,8)$ rotational distributions of the $HeBr_2(B,v=10)$ vibrational predissociation. Vibrational distribution is 97.47%, 2.46%, and 0.06%, for $\Delta v=-1$, -2, and -3, respectively (rotational distribution of $\Delta v=-3$ is not shown here). These results have been obtained within the Golden Rule approach.

	Population (%)		
		Products	
j	Initial state	$v-1$	$v-2$
0	49.16	27.10	24.46
2	35.93	30.10	27.47
4	11.83	18.35	17.90
6	2.58	7.42	8.70
8	0.43	6.09	9.36
10	0.06	6.15	7.90
12	7×10^{-3}	3.43	2.86
14	8×10^{-4}	1.10	0.71
16	8×10^{-5}	0.23	0.39
18	7×10^{-6}	0.04	0.18
$\geqslant20$	$<10^{-6}$	<0.01	<0.10

available energy in the $v=9$ channel (119.01 cm^{-1}). In accordance with experiment, VP of $HeBr_2$ is essentially a V→T process in the low v region (note that for the present situation, rotational channels are open up to $j'=46$).

Table IV also compares the initial quasibound state distributions with the product distributions. The initial state distribution nearly corresponds to a free rotor, i.e., the wave function is quite delocalized in the bending mode, as expected for helium complexes. It is seen that the dynamical process somehow excites the rotational degree of freedom, and thus the validity of a crude sudden approximation is doubtful. On the other hand, the $\Delta v=-1$ product distribution tenuously displays a bimodal structure with a secondary maximum at $j=10$. This structure is also found in the $\Delta v=-2$ channel, with the secondary maximum shifted to $j=8$. Same kind of structures have been previously found both experimental and theoretically for $HeCl_2$,[4] with a rather more pronounced bimodality. The origin of this feature in $HeCl_2$ has been attributed initially to a rotational rainbow effect[34] and later, to a quantum interference effect.[35] For higher levels ($v<39$), rotational distributions are still quite similar to that of $v=10$, although they become more ''statistical'', losing signatures of bimodality. This fact has been observed for $HeCl_2$.[4] Vibrational distributions, on the other hand, change noticeably as Br_2 excitation increases: $\Delta v=-1$ population steadily decreases at the expense of an increase in $\Delta v<-1$ populations. For $v=38$, for example, vibrational distribution is 74.2%, 18.9%, 5.4%, and 1.6% for $\Delta v=-1$, -2, -3, and -4, respectively.

C. High Br_2 vibrational levels: the closing of the $\Delta v=-1$ channel

In Fig. 1 we present a simulation of pump–probe spectra[25] by plotting the $\Delta v=-1,-2$ partial cross sections (summed over all final rotational states) corresponding to excitations to vibrational states $v=42$–46. Figures 1(b) to 1(d), displaying partial cross sections for the outgoing channels $v'=41$ to 44, can be directly compared with the recorded excitation spectra shown in Fig. 5 of Ref. 25. In this section, the partial closing of the $\Delta v=-1$ channel is discussed, together with other interesting effects appearing in the VP of high v states. Before going to a detailed description of Figs. 1(a)–1(d), it is worth noting the rather complicated structures appearing in the cross section profiles. No simple Lorentzian behavior is found for high v levels; instead, the groundlike vdW level at the corresponding v appears to interact rather strongly with several states belonging to the $v'<v$ manifolds.

Figure 1(a) shows the exit through the $v'=41$ channel coming from either $v=42$ ($\Delta v=-1$) or $v=43$ ($\Delta v=-2$). As also occurs at lower v values, the $\Delta v=-1$ dissociation channel yields a more intense peak than the $\Delta v=-2$ one. The same behavior was found in the experimental study.[25] This is the expected situation in VP of vdW complexes, where the propensity rule is that a minimum loss of quantum numbers is the most efficient relaxation channel.[13] However, and in contrast with the experimental finding,[25] the $\Delta v=-2$ transition is more important than the $\Delta v=-1$ one, for the exit through the $v'=42$ channel [see Fig. 1(b)]. This could be due to an effect of partial closing of the $\Delta v=-1$ channel when the $v=43$ state is excited. Comparing Figs. 1(a) and 1(b) for the $v=43$ excitation, it is noticed that the $\Delta v=-2$ cross section is more important than the $\Delta v=-1$ one. This constitutes a novel effect in which, and despite the fact that the $\Delta v=-1$ channel is open, dissociation through $\Delta v=-2$ becomes dominant and therefore an inversion of population is produced. Note that such a situation occurs at very low kinetic energies, ≈3 cm^{-1}, for the new channel is just open. Thus, there is a threshold effect where strong interference among continua belonging to different v' manifolds is expected. The closing of the $\Delta v=-1$ channel becomes evident for the excitation to the $v=44$ state. The most intense peak for the $\Delta v=-2$ transition is found at $E\approx19\,524.9$ cm^{-1}. At this position, the $\Delta v=-1$ channel is still closed [see Fig. 1(c)]. This channel opens at 19 525.1 cm^{-1}, giving rise, in Fig. 1(c), to a small feature peaked at $\approx19\,526$ cm^{-1}, 1.1 cm^{-1} to the blue of the main peak of the $\Delta v=-2$ transition. Also in Fig. 1(c), the partial cross section for dissociation by the $\Delta v=-2$ channel (from $v=45$) exhibits two similar peaks. Since the $\Delta v=-1$ channel from $v=45$ is practically closed [see Fig. 1(d)], the double peak seems to originate from an IVR mechanism wherein at least one bright and one dark states are interacting. Finally, a sharp $\Delta v=-2$ cross section (from $v=46$) is displayed in the right-hand side of Fig. 1(d), where the $\Delta v=-1$ channel is completely closed.

The gradual closing of the $\Delta v=-1$ channel, obtained in our calculations, agrees qualitatively well with the experimental observations [compare Figs. 1(b)–1(d) with Fig. 5 of Ref. 23]. In the experiment, the closing of the $\Delta v=-1$ channel is also found to arise at $v=44$. In addition, the vdW energy at this level, that we assign to the most intense peak in the $\Delta v=-2$ cross section [Fig. 1(b)], is -13.69 cm^{-1} [measured with respect to the $He+Br_2(v=44)$ dissociation

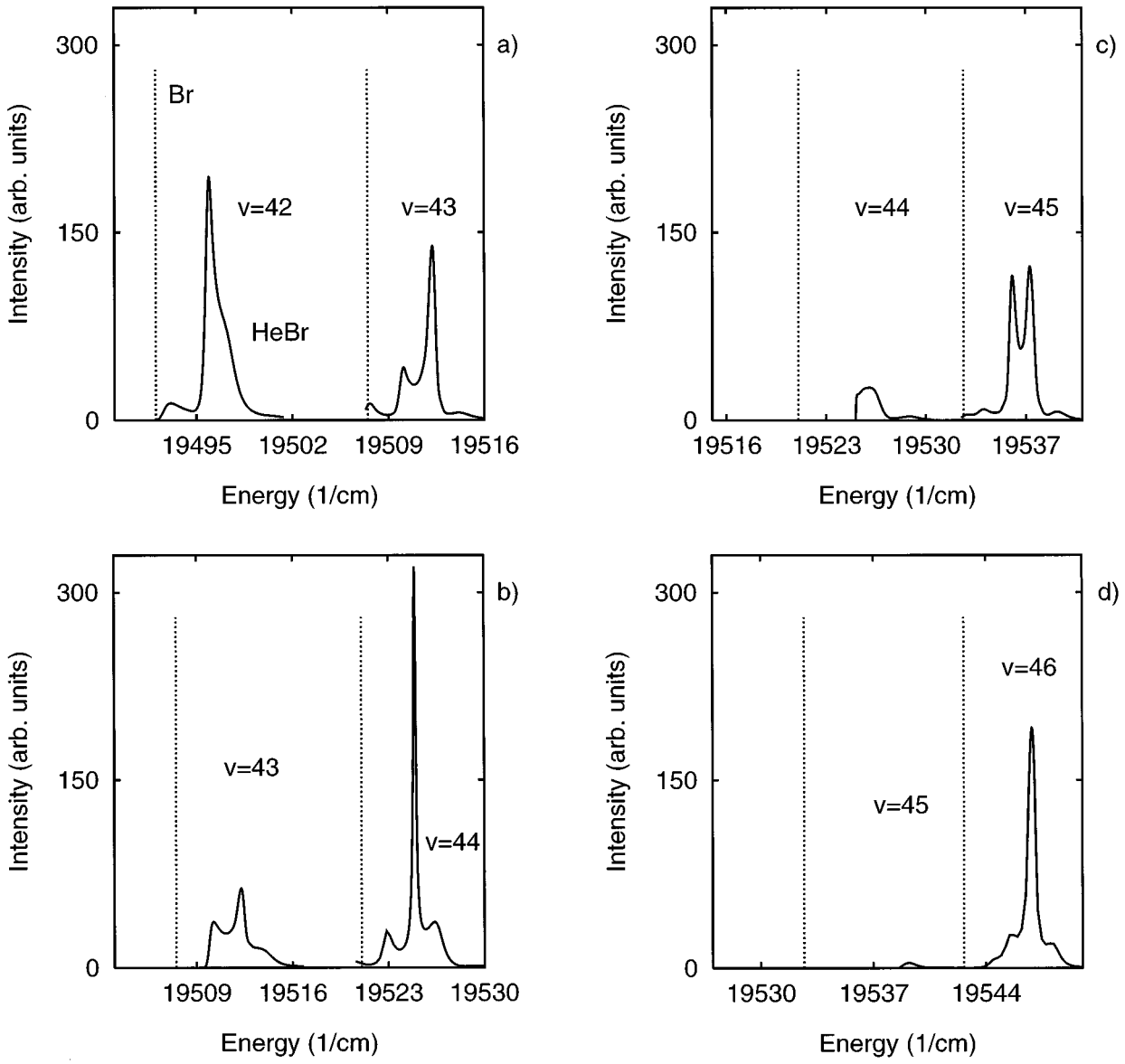

FIG. 1. Simulation of the pump–probe excitation spectra (Ref. 25) for excitation to $v=42$–46 levels. (a) Partial cross section for outgoing channel $v'=41$, when $v=42$ (left) and $v=43$ states (right) are excited. Sticks (in dashed line) indicate the corresponding diatomic transitions followed by vibrational relaxation $Br_2(X, v=0)\rightarrow Br_2(B,v)\rightarrow Br_2(B,v')$. (b) Same for excitations to $v=43$, 44 and exit through $v'=42$. (c) Same for $v=44$, 45, $v'=43$. (d) Same for $v=45$, 46, $v'=44$. Energy (in cm^{-1}) corresponds to the vibronic transition, which equals $T_e-\mathrm{zpe}[Br_2(X)]+D_e[HeBr_2(X)]+E$, where E, referenced to the bottom of the $Br_2(B)$ potential, is varied in the calculations, and $T_e=15\,902.47$ cm^{-1} (Ref. 31), $\mathrm{zpe}[Br_2(X)]=162.39$ cm^{-1}, and $D_e[HeBr_2(X)]=17.57$ cm^{-1}.

threshold]. This magnitude compares quite well with the experimental binding energy, 13.5 ± 1.0 cm^{-1}.[25] The main difference is perhaps that no structured line shapes but rather broad peaks are found in the experiment. It should be recalled that the reported line shapes have been computed for just one rotational transition, whereas in the experiment excitations to several total angular momentum states are involved. The addition of the relevant rotational transitions in the simulated spectra might well lead to a less structured and broader line shape, in better accordance with the experiment.

From these calculations, one sees that the closing of the $\Delta v=-1$ channel is a rather gradual process in which several regimes can be distinguished involving threshold and internal energy redistribution effects. When the $\Delta v=-1$ channel is closed ($v\geqslant 45$), the cross section profiles suggest that an IVR mechanism is taking place. In Fig. 2, the $\Delta v=-2$ rotational distributions for the two most intense resonance peaks are shown. It can be seen that both distributions are rather structured and, besides, fairly similar. This behavior is in accordance with a sparse IVR model where the fragmentation process is mainly dominated by a dark doorway state to which a zero order bright state is coupled.[28] More intriguing is perhaps the existence of complicated structures in the cross section profiles when the $\Delta v=-1$ channel is still open. At $v=43$, rotational distributions for the most intense peaks [see Figs. 1(a) and 1(b)] are quite structured too, but they are not as similar as in the $v=45$ case. Halberstadt *et al.*[28,36] and Roncero *et al.*[37] have carried out theoretical studies on the

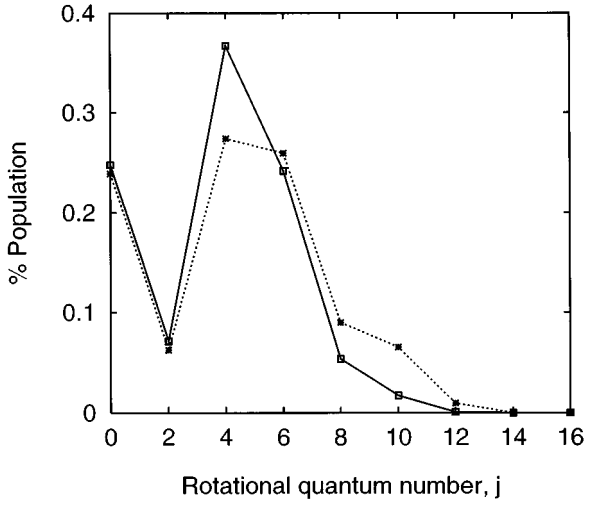

FIG. 2. Solid line: $\Delta v=-2$ rotational $Br_2(B)$ distributions for the $v=45$ excitation, at the peak maximum placed at lower energy in Fig. 1(c) [-14.250 cm^{-1}, with respect to the $He+Br_2(B, v=45)$ threshold]. Dashed line: same for the peak maximum located at higher energy (-13.00 cm^{-1}) in the same figure.

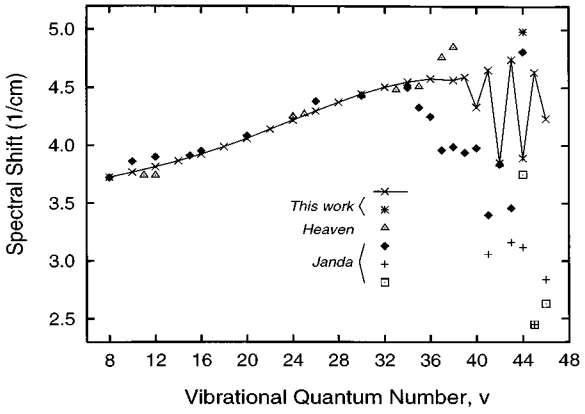

FIG. 3. Calculated spectral shifts (in cm^{-1}) as functions of vibrational excitation v, compared with measured ones. Crosses joined by solid lines are the calculated values. Star indicates the calculated $\Delta v=-1$ blueshift at $v=44$. Open triangles indicate Heaven and co-workers' data (Ref. 24). Filled rhombus, vertical crosses, and open squares correspond to $\Delta v=-1$, $\Delta v=-2$, and $\Delta v=-3$ Janda and co-workers' measurements (Refs. 25 and 26). See the text for more details.

$ArCl_2$ complex, finding that the dissociation dynamics in the $\Delta v=-2$ regime proceeds via IVR in the sparse limit. Very recently, Janda *et al.*[38] have pointed out the appearance of interference effects in the $\Delta v=-1$ regime of $ArCl_2$ due to the existence of long lived resonances (''orbiting'' resonances) in the $v-1$ continuum. It would be very interesting to perform a more detailed study of the threshold and IVR effects in $HeBr_2$ and compare with the $ArCl_2$ dynamics. The lighter mass of He and the smaller vdW well depth in the $HeBr_2$ complex may lead to qualitative differences in the manifestation of such effects. This analysis will be a subject of a forthcoming work.

D. Spectral shifts and linewidths: Comparison with experiment

In this paragraph we summarize the results on spectral shifts and resonance widths for the whole v range studied in this work ($v=8$–46), in comparison with experiment.[24–26]

In Fig. 3, calculated blueshifts $[E_v(B)-E_i(X)]$ are presented and compared with experimental measurements. As can be seen, agreement between experiment and theory is very good up to $v=34$. Above that vibrational excitation, the blueshifts of Jahn *et al.*[25] (obtained using the pump–probe spectroscopic technique) begin to rapidly fall, whereas those of van de Burgt *et al.*[24] (obtained via laser induced fluorescence, LIF) tend to increase as v increases. Jahn *et al.* suggest that the discrepancy between both sets of data is due to the low signal-to-noise ratios found using the LIF technique. Our theoretical shifts, on the other hand, show a plateau in the range $34\leqslant v\leqslant 38$, in between both sets of data. From here on, cross section profiles are no longer Lorentzian. Small deviations from such a behavior are found at $v=39$ and 40. For higher v values, the onset of several other interacting resonances leads to more complicated profiles, as has been already discussed in the previous paragraph. To estimate the corresponding blueshifts, we have considered the position of the most intense peak. In this way, we obtain an oscillatory behavior in the region $39\leqslant v\leqslant 46$. Experimental data also oscillate—dephased from the calculated values—but always remaining below the calculated ones, i.e., measured vdW binding energies in this region are larger than the theoretically estimated ones. Overall, experimental blueshifts tend to decrease as the $Br_2(B)$ dissociation threshold is closer, bearing some resemblance to reported experiments on HeI_2 (Ref. 11). This trend is not evident in the calculations. On the other hand, we do not obtain different blue shifts depending on the exit channel ($\Delta v=-1,-2,...$), as is found experimentally. The only exception concerns the $v=44$ level, where a clear closing of the $\Delta v=-1$ channel is produced and the peaks for $\Delta v=-1$ and $\Delta v=-2$ transitions are located at different excitation energies (see Fig. 1). At this level, we find the following blue shifts: 4.97 cm^{-1} ($\Delta v=-1$), 3.87 cm^{-1} ($\Delta v=-2,-3,-4$), while the experimental work[25] reports 4.81 ± 0.3 ($\Delta v=-1$), 3.12 ± 0.3 ($\Delta v=-2$), 3.75 ± 0.3 ($\Delta v=-3$). For all the other v excitations, it is always found that the main peaks are placed at the same position, regardless of the exit channel v'. Nevertheless, the different Δv blueshifts found in the experiment could be rationalized as follows. For high v values, it is already found that the vibrational populations change dramatically with energy in a small range. In Fig. 4, and for the $v=43$ level, we show the vibrational populations of the different $v'<v$ dissociation channels as functions of energy. The positions of the resonance peaks are also depicted in that figure. Note that if the position of the peaks were shifted, the most populated dissociation channel could differ from one peak to the other. By considering a more accurate potential[26] and taking into account other relevant transitions $J^{p_i}_{p_j}(X)\rightarrow J^{p_i}_{p_j}(B)$, it could certainly happen that the most intense peaks for different Δv dissociation channels are placed at different energy positions, achieving

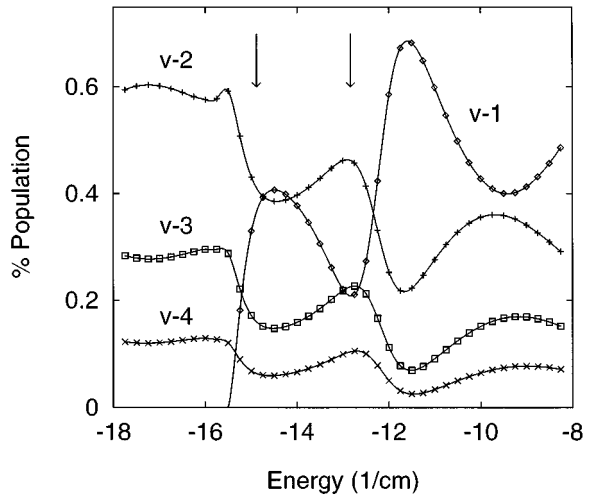

FIG. 4. Product vibrational distribution vs energy (in cm^{-1}) corresponding to excitation of the $v=43$ level. Positions of the main peaks exhibited in the photofragmentation line shape [Figs. 1(a) and 1(b)] are indicated by vertical arrows. Energy is referenced with respect to the $He+Br_2(B, v=43)$ dissociation limit.

in this way a closer agreement with the experimental findings.

Calculated and experimental[24–26] half-widths versus v are presented in Fig. 5. In the region of low v's, where Lorentzian profiles were found, the rates (together with the resonance positions) were calculated by means of fittings to the appropriate analytical functions. For $v \geqslant 38$, where no Lorentzian behavior of the cross sections is encountered, a crude estimation of half-widths at half-maximum (in the blue wing) of the main peak was made. Overall agreement at low v values,[26] intermediate,[24] and high levels[25] up to $v=42$, is achieved. Near the crossover level, $v=44$, as happens for spectral shifts, an oscillatory behavior of the rates appears. This effect, already reported some time ago for related systems such as HeI_2 (Refs. 39 and 40) and NeI_2,[41] can be attributed to the interaction among resonances of different v manifolds, the anharmonicity of the diatomic partner being the ultimate origin of such oscillations. The maximum rate is found at $v=40$, previous to the crossover level $v=44$. This is mainly due to the gradual closing of the $\Delta v=-1$ channel as previously suggested[11] and theoretically obtained[40,41] for He, NeI_2. At $v=44$, as was shown in Fig. 1, a narrow resonance in the $\Delta v=-2$ partial cross section becomes the most intense peak and leads to an unusually long lifetime. Also, the broad feature for $\Delta v=-1$ was found to correspond to a rate of about one half of the experimental value[25] at this level. Finally, at higher initial excitations ($\Delta v=-2$ regime), the calculated half-widths are 3–4 times smaller than those reported by Jahn *et al.*[25]

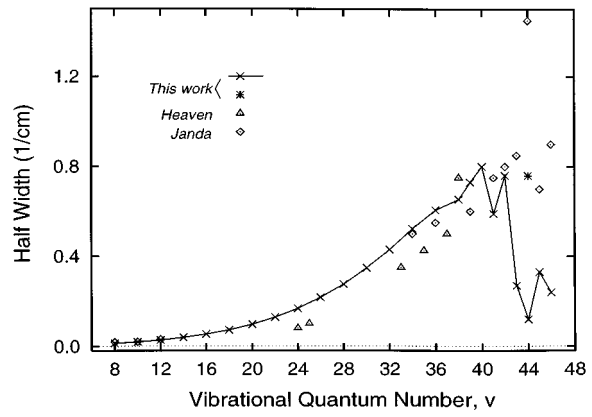

FIG. 5. Calculated half-widths (in cm^{-1}) as functions of the bromine subunit vibrational excitation, compared with measured ones. Crosses joined by solid lines are the calculated values. Star indicates the calculated $\Delta v=-1$ half-width at $v=44$. Open triangles indicate Heaven and co-workers' data (Ref. 24). Open rhombus correspond to Janda and co-workers' measurements (Refs. 25 and 26). See the text for more details.

The discrepancies found when comparing blueshifts and lifetimes with the experimental data in the $v>38$ region might well be due to the fact that the potential model used here is too simplistic. Indeed, it is necessary to carry out more studies on the B state potential when the Br_2 subunit is close to its dissociation limit. Janda and co-workers suggest to build up such an interaction potential starting from the atom–atom potential for the isolated HeBr system.[25] The inclusion of the appropriate long range vdW interaction[26] may also be important since the zero order states which are close to the $He+Br_2(v-1)$ dissociation limit should be very sensitive to the long range details of the interaction; in this way, the manifestation of IVR-like processes could be different. Nonetheless, we think that it would be interesting to study the effect of including other relevant $J^{p_i}_{p_j}(X) \rightarrow J^{p_i}_{p_j}(B)$ transitions, even with the present simple potential model. Since each individual transition yields a complex IVR-like line shape (we have checked this in preliminary calculations), the effect of adding up all these transitions (thus performing a more complete simulation of the spectra) should end up with a less structured and also broader total line shape. The estimation from such spectra of linewidths might lead one to obtain larger ''average'' linewidths than those which we have estimated by looking at just one of the various peaks that the individual transition studied produces.

V. CONCLUDING REMARKS

Three-dimensional quantum mechanical calculations have been carried out to study the vibrational predissociation of the $HeBr_2$ molecule over a wide range of initial Br_2 vibrational excitations ($v=8$–46). For both X and B electronic states, simple additive He–Br Morse potentials have been proposed to simulate the fragmentation dynamics. At low v values, calculated linewidths and blueshifts are compared with those obtained by means of simpler Golden Rule calculations and also, with previously published calculations[26] where somewhat different interaction potentials were employed. When comparing with experiments, the potential model used in this work successfully reproduces the (X, $v=0$) vdW binding energy, the (X, $v=0$) and (B, $v=8$) average structures, the average product energies (B, $v=10$) and, at $v=44$, the closing of the $\Delta v=-1$ channel and the B

state binding energy. In addition, spectral shifts and linewidths agree satisfactorily well with the measured ones up to $v \approx 38$. For higher v excitations, calculated shifts are above reported data, whereas linewidths fall well below the measured values. Another aspect which theory cannot reproduce satisfactorily with the present potential model is the experimental observation of a bending excitation band at $v=8$. It is clear that further investigations on the B state potential are needed, to account for the excited vdW mode bands as well as the surprisingly small spectral shifts at excitations near the $Br_2(B)$ dissociation limit.

On the other hand, the calculated cross section profiles and product distributions suggest the onset of important energy redistribution and threshold interference effects in the high v region. It has been shown that by varying the v excitation, different dynamical regimes are probed. In this sense, recent research on the $ArCl_2$ complex has provided interesting conclusions.[6,28,36–38] Since the vdW dissociation energy is smaller in the $HeBr_2$ system than in $ArCl_2$, the closing of the $\Delta v=-1$ channel occurs at higher $Br_2(v)$ excitations. The intramolecular dynamics might show different effects when the halogen subunit is near dissociation. In would be interesting to check these predictions with experiments, either in the time[42,43] or in the energy[6] domain. In the latter case, achievement of resolved product distributions would help to elucidate the details of $HeBr_2$ dissociation dynamics. On the theoretical side, and in order to better compare with reported experiments, it would be convenient to carry out a more complete calculation of the excitation spectra, by taking into account the relevant rotational transitions for a given beam temperature. To attain a more accurate picture of the $HeBr_2$ intramolecular dynamics, approaches within time-dependent wave packet schemes[37,44] or quasibound state analysis[36] can be helpful. In this last avenue, stabilization calculations[45,46] could be insightful. Work in these directions is in progress.

ACKNOWLEDGMENTS

We are deeply grateful to K. C. Janda for providing us with results prior to publication. Also, we thank O. Roncero, N. Halberstadt, and J. A. Beswick for very helpful and illuminating discussions. This work has been supported by the D.G.I.C.Y.T. Grant PB95-0071 (Spain), and the INTAS-93-1809 and CI1*-CT94-0128 Grants (European Union).

[1] R. E. Smalley, D. H. Levy, and L. Wharton, J. Chem. Phys. **64**, 3266 (1976).
[2] R. E. Smalley, L. Wharton, and D. H. Levy, J. Chem. Phys. **68**, 671 (1978).
[3] J. A. Blazy, B. M. DeKoven, T. D. Russell, and D. H. Levy, J. Chem. Phys. **72**, 2439 (1980).
[4] J. I. Cline, B. P. Reid, D. D. Evard, N. Sivakumar, N. Halberstadt, and K. C. Janda, J. Chem. Phys. **89**, 3535 (1988).
[5] D. D. Evard, F. Thommen, and K. C. Janda, J. Phys. Chem. **91**, 2508 (1987).
[6] D. D. Evard, C. R. Bieler, J. I. Cline, N. Sivakumar, and K. C. Janda, J. Chem. Phys. **89**, 2829 (1988).
[7] J. M. Skene and M. I. Lester, Chem. Phys. Lett. **116**, 93 (1985).
[8] J. M. Skene, J. C. Drobits, and M. I. Lester, J. Chem. Phys. **85**, 2329 (1986).
[9] R. L. Waterland, M. I. Lester, and N. Halberstadt, J. Chem. Phys. **92**, 4261 (1990).
[10] J. A. Beswick and G. Delgado-Barrio, J. Chem. Phys. **73**, 3653 (1980).
[11] W. Sharfin, P. Kroger, and S. C. Wallace, Chem. Phys. Lett. **85**, 81 (1982).
[12] J. A. Beswick and J. Jortner, Adv. Chem. Phys. **47**, 363 (1981).
[13] G. E. Ewing, J. Phys. Chem. **91**, 4662 (1987).
[14] G. Delgado-Barrio, in *Dynamical Processes in Molecular Physics*, edited by G. Delgado-Barrio (IOP, Bristol, 1993).
[15] G. Delgado-Barrio, S. Serna, S. Miret-Artés, O. Roncero, J. Campos-Martínez, and P. Villarreal, Laser Chem. **12**, 103 (1992), and references therein.
[16] N. Halberstadt, J. A. Beswick, and K. C. Janda, J. Chem. Phys. **87**, 3966 (1987).
[17] O. Roncero, J. A. Beswick, N. Halberstadt, P. Villarreal, and G. Delgado-Barrio, J. Chem. Phys. **92**, 3348 (1990).
[18] F. M. Tao and W. Klemperer, J. Chem. Phys. **97**, 440 (1992).
[19] J. Sadlej, G. Chalasinski, and M. M. Szczesniak, J. Chem. Phys. **99**, 3700 (1993).
[20] G. Chalasinski, M. Gutowski, M. M. Szczesniak, J. Sadlej, and S. Scheiner, J. Chem. Phys. **100**, 6800 (1994).
[21] S. S. Huang, C. R. Bieler, K. C. Janda, F. Tao, W. Klemperer, P. Casavecchia, G. Volpi, and N. Halberstadt, J. Chem. Phys. (to be published).
[22] L. Beneventi, P. Casavecchia, G. Volpi, C. R. Bieler, and K. C. Janda, J. Chem. Phys. **98**, 178 (1993).
[23] A. A. Buchachenko and N. F. Stepanov, J. Chem. Phys. (in press), and references therein.
[24] L. J. van de Burgt, J. P. Nicolai, and M. C. Heaven, J. Chem. Phys. **81**, 5514 (1984).
[25] D. G. Jahn, S. G. Clement, and K. C. Janda, J. Chem. Phys. **101**, 283 (1994).
[26] D. G. Jahn, W. S. Barney, J. Cabalo, S. G. Clement, T. J. Slotterback, K. C. Janda, and N. Halberstadt, J. Chem. Phys. **104**, 3501 (1996).
[27] N. Sivakumar, J. I. Cline, C. R. Bieler, and K. C. Janda, Chem. Phys. Lett. **147**, 561 (1988).
[28] N. Halberstadt, J. A. Beswick, O. Roncero, and K. C. Janda, J. Chem. Phys. **96**, 2404 (1992).
[29] L. Fox, *The Numerical Solution of Two-Point Boundary Value Problems in Ordinary Differential Equations* (Oxford University Press, London, 1957).
[30] O. Roncero (private communication).
[31] K. P. Huber and G. Herzberg, *Constants of Diatomic Molecules* (van Nostrand Reinhold, New York, 1979).
[32] R. F. Barrow, T. C. Clark, J. A. Coxon, and K. K. Yee, J. Mol. Spectrosc. **51**, 428 (1974).
[33] As is stated in Ref. 25 (footnote 43 therein), the linewidths (FWHM) reported by van der Burgt *et al.* (Ref. 24) were twice the actual linewidths.
[34] N. Halberstadt, R. Schinke, and J. A. Beswick, in AIP Conf. Proc. **225** (AIP, New York, 1991).
[35] S. K. Gray, and C. E. Wozny, J. Chem. Phys. **94**, 2817 (1991).
[36] N. Halberstadt, S. Serna, O. Roncero, and K. C. Janda, J. Chem. Phys. **97**, 341 (1992).
[37] O. Roncero, P. Villarreal, G. Delgado-Barrio, N. Halberstadt, and K. C. Janda, J. Chem. Phys. **99**, 1035 (1993).
[38] K. C. Janda, N. Halberstadt, and O. Roncero (unpublished).
[39] P. Villarreal, G. Delgado-Barrio, P. Mareca, and J. A. Beswick, J. Mol. Struct. **120**, 303 (1985).
[40] G. Delgado-Barrio, P. Villarreal, P. Mareca, and J. A. Beswick, Int. J. Quantum Chem. **27**, 173 (1985).
[41] O. Roncero, J. Campos-Martínez, A. M. Cortina, P. Villarreal, and G. Delgado-Barrio, Chem. Phys. Lett. **148**, 62 (1988).
[42] J. J. Breen, D. M. Willberg, M. Gutmann, and A. H. Zewail, J. Chem. Phys. **93**, 9180 (1990).
[43] M. Gutmann, D. M. Willberg, and A. H. Zewail, J. Chem. Phys. **97**, 8048 (1992).
[44] O. Roncero and S. K. Gray, J. Chem. Phys. **104**, 4999 (1996).
[45] V. A. Mandelshtam, T. R. Ravuri, and H. S. Taylor, Phys. Rev. Lett. **70**, 1932 (1993).
[46] M. I. Hernández and D. C. Clary, J. Chem. Phys. **101**, 2779 (1994).